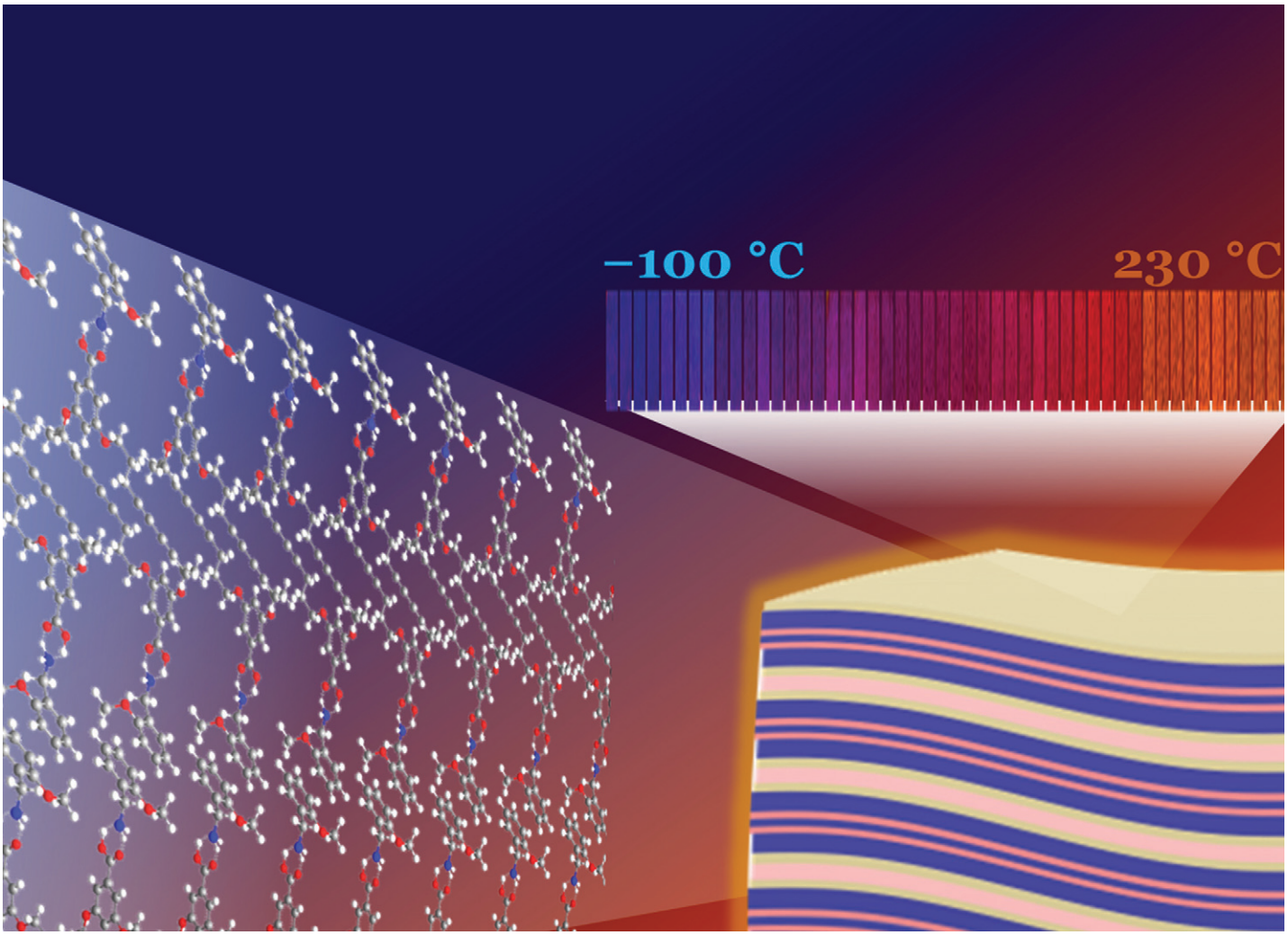

Showcasing research from Professor Oaki's laboratory, Department of Applied Chemistry, Faculty of Science and Technology, Keio University, Yokohama, Japan.

Layered macrocycles with flexibility and tunable dynamic properties for wide-range thermoresponsive color changes

Layered macrocycles have been designed and introduced as a new family of layered materials. A macrocycle containing functional, flexibility, and intercalating units forms layered materials with structural flexiblity and tunable dynamic properties. The flexible layered macrocycles containing intrinsically rigid π-conjugated moiety exhibited thermoresponsive color changes in a wide temperature range of −100 to 230 °C with tunability and reversibility. The paper-based device of the layered macrocyclic polydiacetylene was applied to real-time visualization of temperature distribution on cryotherapy using liquid nitrogen.

As featured in:

See Jong-Man Kim, Yuya Oaki *et al.*, *Sens. Diagn.*, 2022, **1**, 160.

ROYAL SOCIETY OF CHEMISTRY

rsc.li/sensors

Registered charity number: 207890

Sensors & Diagnostics

PAPER

View Article Online
View Journal | View Issue

Cite this: *Sens. Diagn.*, 2022, **1**, 160

Layered macrocycles with flexibility and tunable dynamic properties for wide-range thermoresponsive color changes†

Nano Shioda,[a] Jung-Moo Heo,[b] Bubsung Kim,[b] Hiroaki Imai,[a] Jong-Man Kim *[b] and Yuya Oaki *[a]

Layered materials exhibit unique properties, such as intercalation and exfoliation, originating from the two-dimensional anisotropic nanostructures. A variety of inorganic and organic layered materials have been synthesized for design of functions. However, conventional host layers are static and rigid to induce dynamic functions originating from the structural flexibility. The present work shows a new dynamic and flexible host layer based on organic macrocycles. A macrocycle containing functional, flexible, and intercalating units, namely macrocyclic diacetylene (MCDA), was designed to form a self-assembled layered structure. After the guest molecules were intercalated in the interlayer space, the host MCDA layers were topochemically polymerized to obtain polydiacetylene. The layered macrocycles containing the π-conjugated main chain and interlayer guests showed gradual thermoresponsive color changes in a wide temperature range of −100 to 230 °C with variation of the effective conjugation length. The flexible host layer affords induction of the dynamic motion of the intrinsically rigid π-conjugated main chain in the wide temperature range. Moreover, the thermo-responsivity was tuned by the intercalated guests. The color-change properties enabled real-time temperature imaging for medical applications. Flexible layered macrocycles can be a new design strategy of soft materials with dynamic functions.

Received 24th September 2021,
Accepted 1st November 2021

DOI: 10.1039/d1sd00024a

rsc.li/sensors

Introduction

Layered structures are found in a variety of materials, such as inorganic, organic, hybrid, and polymeric materials.[1–11] Two-dimensional (2D) functional nanoarchitectures are designed and derived from layered materials through intercalation, exfoliation, and self-assembly.[11–22] The host layers generally comprise 2D molecular networks based on covalent bonding and/or noncovalent interaction. The unit layers require an appropriate rigidity to preserve the 2D anisotropic structures. Therefore, it is not easy to prepare flexible host layers exhibiting dynamic properties. The present work shows a new type of flexible layered material based on macrocycles, its intercalation behavior, and dynamic properties (Fig. 1). In previous work, dynamic functions of organic layered materials were observed on smectic liquid crystals and self-assembled lamellar structures.[7,9,23–27] However, stacking of the rigid mesogenic parts and/or assembly of structure-directing alkyl chains lowers the flexibility. In addition, dynamic motion of the functional π-conjugated frameworks is not easily achieved because of their rigidity and stacking nature. Here we designed a macrocycle forming the layered structure with tunable dynamic properties (Fig. 1). The macrocycle, namely macrocyclic diacetylene (MCDA), comprises three units, *i.e.* functional, flexible linker, and intercalating units (Fig. 1a). The diacetylene (DA) moiety as the functional unit provides the π-conjugated polydiacetylene (PDA) main chain exhibiting stimuli-responsive color-change properties. In addition, an appropriate rigidity is ensured to preserve the layered assembly with stacking and linking of the macrocycles (Fig. 1b–e). The linker provides the structural flexibility and stability of the functional units originating from the conformational diversity and cross-linkage, respectively. When the functional units are rigid π-conjugated parts, the flexibility is particularly important to induce the dynamic motion. In addition to the flexibility, the original self-assembled structures are stabilized by the linkers forming the macrocycles. The interlayer space for accommodation of the guests is generated by the carboxy group as the intercalating unit (Fig. 1b–d). The structure flexibility can be tuned by intercalation of the guest molecules and ions. Therefore, the layered MCDA has

[a] *Department of Applied Chemistry, Faculty of Science and Technology, Keio University, 3-14-1 Hiyoshi, Kohoku-ku, Yokohama 223-8522, Japan.*
E-mail: oakiyuya@applc.keio.ac.jp
[b] *School of Chemical Engineering, Hanyang University, Seoul 04763, Korea.*
E-mail: jmk@hanyang.ac.kr

† Electronic supplementary information (ESI) available: Experimental methods, intercalation behavior, and color-change properties. See DOI: 10.1039/d1sd00024a

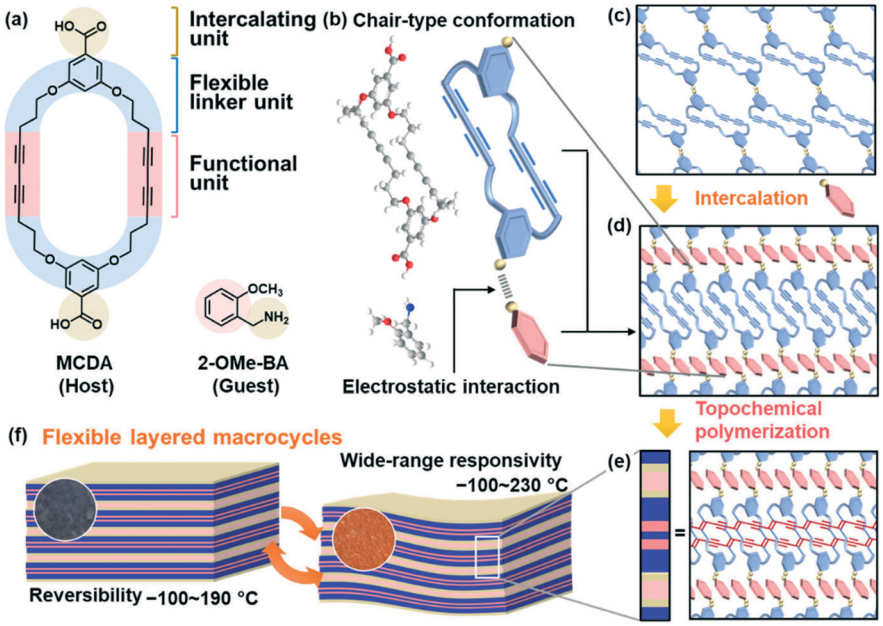

Fig. 1 Schematic illustrations of the layered macrocycles and their flexible polymers. (a and b) Molecular structures (a) and conformations (b) of the host MCDA and guest 2-OMe-BA. (c) Layered structure of MCDA. (d and e) Layered structures of MCDA-(2-OMe-BA) (d) and PMCDA-(2-OMe-BA) with topochemical polymerization (e). (f) Layered structure of PMCDA-(2-OMe-BA) with wide-range thermoresponsive and reversible color-changing properties (light yellow: intercalating units with electrostatic interaction between carboxy and amino groups, dark blue: flexible linker units preserving the layered structures, red: PDA main chains as the functional units, pink: intercalated guests).

potential for tunable and unique dynamic properties originating from the intercalation capability and structure flexibility (Fig. 1b–e). The conjugated PDA main chain in the layered MCDA and interlayer guest exhibited gradual thermoresponsive color changes in a wide temperature range of −100 to 230 °C with tunability and reversibility (Fig. 1f). The structure flexibility originating from the layered macrocycles plays an important role in the emergence of the dynamic properties based on the rigid π-conjugated parts. The design strategy of layered macrocycles can be applied to development of diverse soft π-conjugated materials.

PDA exhibits stimuli-responsive color changes with molecular motion and subsequent variation of the effective conjugation length.[28–38] DA moieties with a distance shorter than 0.5 nm are topochemically polymerized in the condensed states with irradiation of UV light.[39] A wide variety of DA monomers and their assembled structures have been studied for control of the stimuli responsivity toward sensing applications.[40–51] The macrocycles containing DA moieties have been synthesized to obtain the self-assembled tubular PDA exhibiting thermochromism and solvatochromism.[52–55] However, control of the stimuli responsivity and structural flexibility is not easily achieved only by the molecular design. Another approach to control the stimuli responsivity is intercalation of the guest ions and molecules in the interlayer space of layered PDA.[56–60] An amphiphilic DA monomer, such as 10,12-pentacosadiynoic acid (PCDA), forms the lamellar crystal structure with the interlayer space consisting of dimerized carboxy groups. However, the flexibility of the layered structures is not fully derived from changes in the intercalated guests because the rod-like host and guest molecules form the densely packed assembly *via* van der Waals interaction. If more flexible layered structures are designed, the range of the stimuli responsivity can be widened by the dynamic motion of the intrinsically rigid PDA main chain. Therefore, we designed a new MCDA forming the layered structures with flexibility and intercalation capabilities.

Results and discussion

Intercalation chemistry of layered macrocycles

MCDA was synthesized according to literature procedures (Scheme S1 and Fig. S1 in the ESI†).[52,61] The powder of MCDA, 5 mg (8.8×10^{-3} mmol), was dispersed in 0.5 cm^3 purified water. After 0.5 cm^3 purified water and 8.8×10^{-3} mmol organic amines, such as benzyl and alkyl amines (Fig. S2 in the ESI†), were added, the dispersion liquid was maintained for 1 h in a sonic bath. The precipitate was collected, rinsed with purified water, and then dried at room temperature. The detailed methods are described in the ESI.† Cationic organic amines, such as 2-methoxybenzylamine (2-OMe-BA), were introduced in the interlayer space (Fig. 2 and S2 and S3 in the ESI†). Here the intercalation of 2-OMe-BA and its polymerization behavior was described as a representative result.

The precursor MCDA showed the absorption peak corresponding to the C═O stretching vibration of the intermolecular dimerized carboxy groups at around 1700 cm^{-1} in the Fourier-transform infrared (FT-IR) spectrum

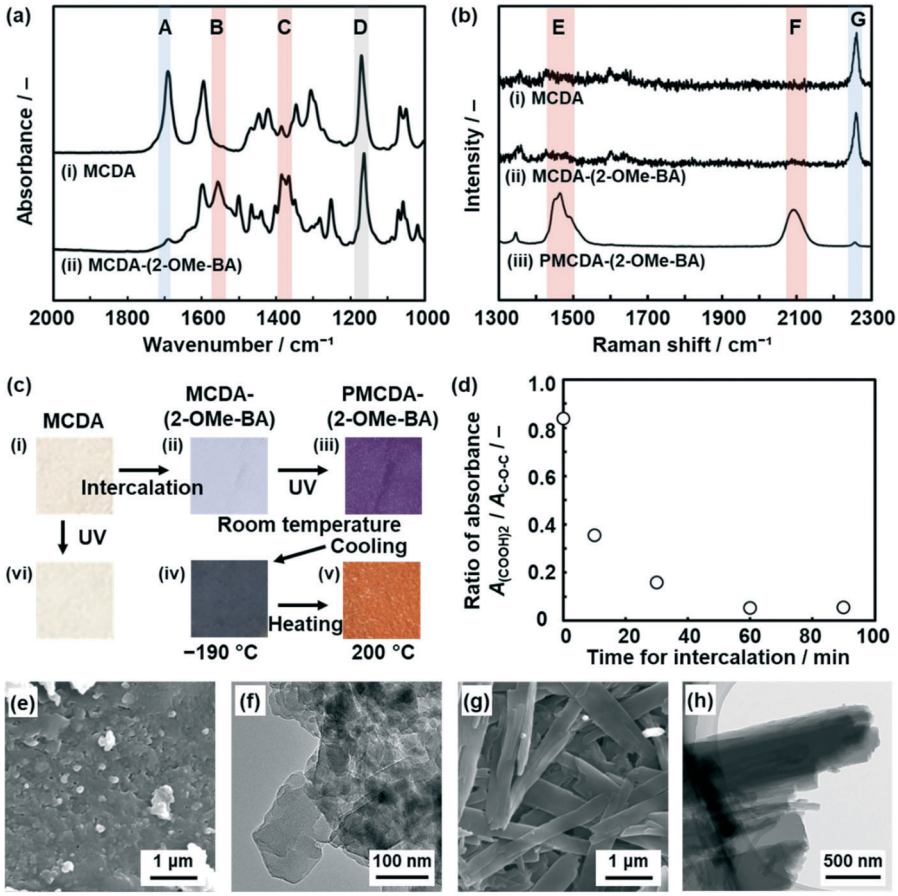

Fig. 2 Intercalation and polymerization behavior of the layered macrocycles. (a) FT-IR spectra of MCDA (i) and MCDA-(2-OMe-BA) (ii). (b) Raman spectra of MCDA (i), MCDA-(2-OMe-BA) (ii), and PMCDA-(2-OMe-BA) (iii). (c) Photographs of MCDA (i), MCDA-(2-OMe-BA) (ii), PMCDA-(2-OMe-BA) (iii–v) at room temperature (iii), −190 °C (iv), 200 °C (v), and MCDA with irradiation of UV (vi). (d) Relationship between time for the intercalation and $A_{(COOH)2}/A_{C-O-C}$. (e–h) SEM (e and g) and TEM (f and h) images of MCDA (e and f) and PMCDA-(2-OMe-BA) after the intercalation for 60 min (g and h).

(band A in spectrum (i) in Fig. 2a). On the other hand, the peaks corresponding to the monomeric carboxylate group appeared at around 1550 cm^{-1} and 1400 cm^{-1} for the layered composites of MCDA and 2-OMe-BA (MCDA-(2-OMe-BA)) (bands B and C in spectrum (ii) in Fig. 2a), even though the weak original peak corresponding to the dimerized carboxy group remained. All the other peaks were assigned to the molecular structures of MCDA and 2-OMe-BA (Fig. S4 in the ESI†).

According to the X-ray diffraction (XRD) pattern, the interlayer distance was shifted from 1.41 nm for MCDA to 1.92 nm for MCDA-(2-OMe-BA) (Fig. S5 in the ESI†). CHN elemental analysis indicates that the molar ratio of MCDA : 2-OMe-BA was calculated to be 1.00 : 1.68. The ideal molar ratio of MCDA : 2-OMe-BA is 1 : 2 on the assumption that the guest is fully intercalated with the bilayer interdigitated state, namely an occupancy of 100% as shown in Fig. 1b and d. Therefore, the occupancy of the guests was 84% to the host MCDA. As the remaining original peak corresponding to the dimerized carboxy groups disappeared with the prolongation of the intercalation time for 90 min (Fig. S6 in the ESI†), the occupancy reached 100%.

The resultant MCDA-(2-OMe-BA) was polymerized with irradiation of a UV-LED at 265 nm for 1 min at 20 °C. Raman spectroscopy of MCDA and MCDA-(2-OMe-BA) showed a peak at around 2260 cm^{-1} assignable to the C≡C group of the DA moiety (band G in spectra (i) and (ii) in Fig. 2b). After the polymerization, the Raman bands corresponding to the ene–yne structure in the PDA main chain appeared at around 1500 and 2100 cm^{-1} (bands E and F in spectrum (iii) in Fig. 2b). The original color of MCDA and MCDA-(2-OMe-BA) was white (images (i) and (ii) in Fig. 2c). The color of the polymerized MCDA-(2-OMe-BA) (PMCDA-(2-OMe-BA)) was reddish purple at room temperature, blue at −190 °C with cooling, and orange at 200 °C with heating (images (iii)–(v) in Fig. 2c). The coloration with irradiation of UV light corresponds to the formation of the PDA main chain with polymerization of MCDA. The thermoresponsive color change originates from the shortening of the effective conjugation length of the PDA main chain with molecular motion in response to thermal stress. These color changes are characteristic of PDA. In contrast, MCDA itself was not polymerized with irradiation of UV light under the same conditions because the characteristic coloration and its

thermoresponsive changes were not observed (image (vi) in Fig. 2c). In general, topochemical polymerization proceeds in the condensed states when DA moieties are arranged with a distance shorter than 0.5 nm.[39] The DA moieties are not arranged for the topochemical polymerization in the layered structure of the pure MCDA (Fig. 1c and S5 in the ESI†). The intercalation of 2-OMe-BA changes the self-assembled layered structure enabling the topochemical polymerization (Fig. 1c–e).

The intercalation and polymerization behavior were studied using different guest amines (Fig. S2 and S3 in the ESI†). The blue-color PMCDAs were obtained by topochemical polymerization when the following amines, such as benzylamine and thiophene derivatives, were intercalated: benzylamine (BA), 4-methylbenzylamine (Me-BA), 4-fluorobenzylamine (F-BA), 3-OMeBA, 4-OMeBA, *m*-xylylenediamine (*m*-Xy), *p*-xylylenediamine (*p*-Xy), and 3-thiophenemethylamine (Tp-CH_2NH_2). These small guest molecules form the topochemically polymerizable self-assembled layered structures (Fig. 1d). On the other hand, red-color PMCDAs were observed with intercalation of more bulky and aliphatic amines, such as hexylamine, 3-phenylpropylamine, and 1-naphthylmethylamine (Fig. S2 and S3 in the ESI†). In these cases, the DA moieties are not self-assembled with the intercalation of the bulky guests. In this manner, the topochemically polymerizable layered structures are obtained by the intercalation of the smaller guest molecules.

The intercalation of the guest in the layered MCDA gradually proceeded within 60 min (Fig. 2d and S6 in the ESI†). The time for the intercalation of 2-OMe-BA was changed to be 10, 30, 60, and 90 min. When the cationic guest is intercalated in the interlayer space, the interlayer dimerized carboxy group is changed to the carboxylate one. In the FT-IR spectra, the absorbance corresponding to the stretching vibrations of the dimerized carboxy groups ($A_{(COOH)2}$, peak A in Fig. 2a) decreased compared with that of the C–O–C bond in the MCDA ring (A_{C-O-C}, peak D in Fig. 2a). The ratio of the absorbance ($A_{(COOH)2}/A_{C-O-C}$) represents the intercalation rate (Fig. 2d). The time-

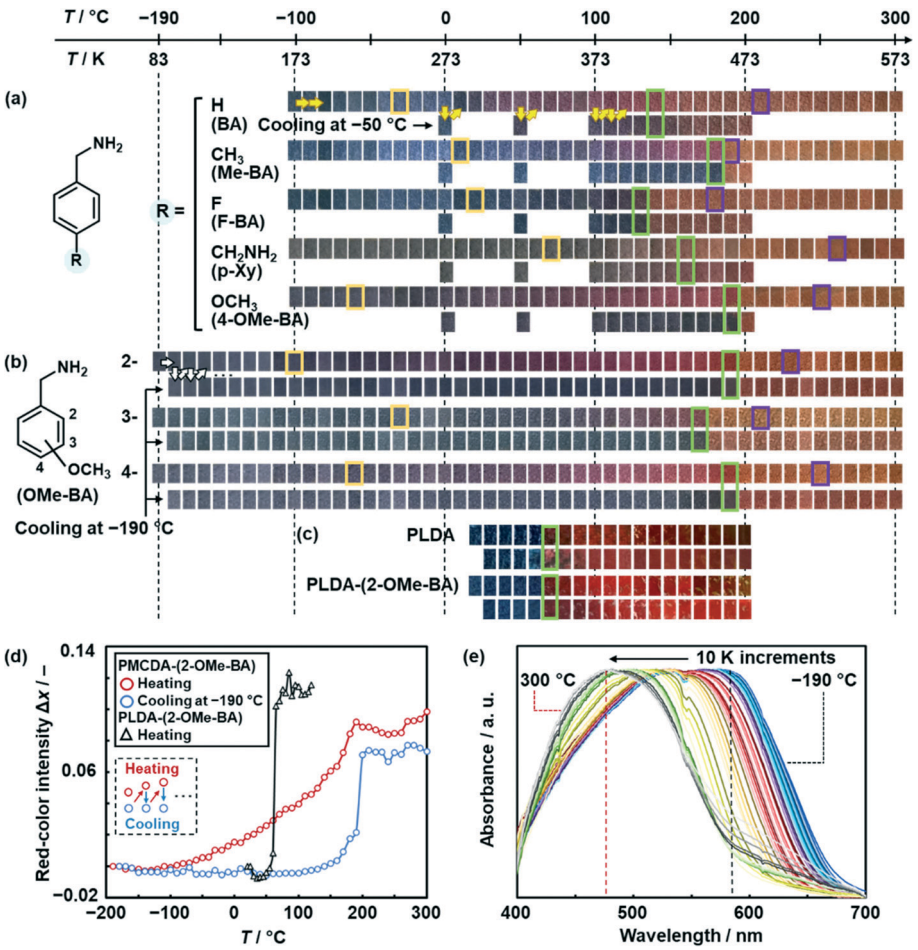

Fig. 3 Thermoresponsive color-changing properties. (a) Color-change behavior of PMCDA series with repetitive heating at a certain temperature and subsequent cooling at −50 °C, as indicated by the arrows. (b) Color-change behavior of PMCDA-(2-OMe-BA), PMCDA-(3-OMe-BA), and PMCDA-(4-OMe-BA) with repetitive heating and subsequent cooling at −190 °C. (c) Color-change behavior of PLDA and PLDA-(2-OMe-BA) as the references. (d) Relationship between T and Δx of PMCDA-(2-OMe-BA) with heating (red) and cooling at −190 °C (blue) and PLDA-(2-OMe-BA) (black). (e) Temperature-dependent changes of UV-vis spectra of PMCDA-(2-OMe-BA) with heating from −190–300 °C.

dependent changes in $A_{(COOH)2}/A_{C-O-C}$ indicate that the intercalation of 2-OMe-BA gradually proceeded and completed within 60 min. Whereas aggregates of nanoflakes around 100 nm in size were observed on the precursor MCDA by scanning electron microscopy (SEM) and transmission electron microscopy (TEM) (Fig. 2e and f), PMCDA-(2-OMeBA) showed nanoribbons *ca.* 500 nm in width and several micrometers in length after the intercalation of the guests for 60 min (Fig. 2g and h). The ratio of the nanobelts increased with the prolongation of the time for the intercalation (Fig. S6 in the ESI†). Nanoribbons were observed in the TEM image of the MCDA-(2-OMe-BA) sample before the polymerization (Fig. S7 in the ESI†). The morphology change implies that the intercalation of the guests induces large structural changes originating from the flexibility of the macrocycles, such as conformation and packing state (Fig. 1c and d).

Wide-range thermoresponsive color-change properties with reversibility

The color of the layered PMCDA with intercalation of the guests was gradually changed with heating in a wide temperature range (Fig. 3a and b). The upper and lower rows of each sample show the colors with heating at a certain temperature and cooling at −50 or −190 °C, respectively (Fig. 3a and b). PMCDA with intercalation of BA, Me-BA, F-BA, *p*-Xy, and 4-OMe-BA exhibited thermoresponsive gradual color changes from blue to orange *via* purple and red in a wide temperature range (the upper rows in Fig. 3a). The reversibility of the color changes was partially observed with cooling at −50 °C in a certain temperature range (the lower rows in Fig. 3a). The color-changing properties, such as temperature responsivity and reversibility, depended on the guests. As the color-changing temperature range of 4-OMe-BA was the widest, the effects of the isomers on the responsivity were studied using 2-, 3-, and 4-OMe-BA in the wider temperature range of −190–300 °C (Fig. 3b). The widest thermoresponsivity in the range of −100–230 °C and reversibility in the range of −100–100 °C were observed for PMCDA-(2-OMe-BA) (Fig. 3b). Thermogravimetric (TG) analysis indicates that the disappearance of thermoresponsivity and reversibility corresponds to the combustion of the host MCDA and volatilization of the guest 2-OMe-BA with deintercalation, respectively (Fig. S8 in the ESI†). Nanograins were formed inside of the PMCDA-(2-OMe-BA) nanoribbons with cracking after the color changes with heating at 200 °C (Fig. 1c and S7 in the ESI†). The reference layered PDA was prepared with a linear DA (LDA) monomer.[58] The polymerized LDA (PLDA) with the intercalation of organic amines showed a similar morphology variation after the color changes with heating in our previous work.[57] The elimination of the guests from the host layered PDA causes the morphology changes with volume shrinkage. Moreover, the reversibility of the color changes between −100 and 100 °C was stably observed for 10 cycles and after the long-term heating for 1 h (Fig. S8 in the ESI†). The color changes were achieved in real time within 0.1 s upon changes in temperature (Fig. S9 in the ESI†). The PLDA with intercalation of the guests were obtained by topochemical polymerization. The initial blue color of the layered PLDA without the interlayer guests and with 2-OMe-BA irreversibly turned red at the threshold temperature of around 65 °C (Fig. 3c). Although the color-transition temperature varied depending on the types of the guests (Fig. 3c and S10 in the ESI†), the wide-range thermoresponsive gradual color changes were not observed for the PLDA series.

The color-change properties were quantitatively characterized by image analysis of the photographs and UV-vis spectroscopy (Fig. 3d and e and S11 in the ESI†). The red-color intensity (x) was estimated from the R, G, and B values of the photographs using an international standard, namely ITU-R BT. 709.[62] The differences in x ($\Delta x = x - x_0$) were calculated from x at varied temperature and x at the initial temperature (x_0), such as −190 °C for the PMCDA series and 20 °C for the PLDA series. The relationship between temperature (T) and Δx was determined with repetitive heating at a certain temperature and subsequent cooling at −190 °C (Fig. 3d and S11 in the ESI†). Whereas the Δx of PMCDA-(2-OMe-BA) gradually increased with heating (red circles in Fig. 3d), PLDA-(2-OMe-BA) showed the transition of Δx at the threshold temperature (black triangles in Fig. 3d). The Δx values of PMCDA-(2-OMe-BA) recovered with heating followed by cooling at −190 °C (blue circles in Fig. 3d). Whereas the other PMCDA series with intercalation of BA, Me-BA, F-BA, *p*-Xy, and 4-OMe-BA also showed similar thermoresponsive gradual color changes with partial reversibility, the color transition at the threshold temperature was observed for the PLDA series (Fig. S9 and S10 in the ESI†). The starting (T_{start}) and ending (T_{end}) temperatures of the color change, upper temperature limit of the reversibility (T_{rev}), and temperature range of the reversibility (ΔT_{rev}) were defined and calculated from the relationship between T and Δx for the layered PMCDA and PLDA series (Table 1 and Fig. S11 in the ESI†). The photographs corresponding to T_{start}, T_{end}, and T_{rev} were surrounded by yellow, purple, and green, respectively in Fig. 3a–c. These results indicate that the PMCDA series exhibits a wider color-change temperature range with partial reversibility compared with the PLDA series. The temperature range for the color changes of PMCDA-(2-OMe-BA) is the widest

Table 1 Summary of T_{start}, T_{end}, T_{rev}, and ΔT_{rev} of the PMCDA series with intercalation of the different guests

Guests	T_{start}/°C	T_{end}/°C	T_{rev}/°C	ΔT_{rev}/K
BA	−40	210	140	180
Me-BA	10	190	180	170
F-BA	20	180	130	110
p-Xy	70	260	160	90
2-OMeBA	−100	230	190	290
3-OMeBA	−30	210	170	200
4-OMeBA	−60	250	190	250

for thermoresponsive color-changing materials containing rigid π-conjugated chromophores in previous studies (Fig. S12 in the ESI).[56,58,59,61,63–67]

The UV-vis spectra indicate the gradual motion of the π-conjugated main chain originating from the flexibility (Fig. 3e). The UV-vis spectrum of PMCDA-(2-OMe-BA) was gradually shifted from 585 nm at −190 °C to 480 nm with heating to 300 °C (Fig. 3e). The spectra with heating below 110 °C recovered to the original position after cooling at −190 °C (Fig. S13 in the ESI†). The reversibility was gradually decreased after the heating in the range of 110–190 °C (Fig. S13 in the ESI†).

The thermal motion of the layered structures induces the torsion of the PDA main chain. The color is changed with shortening of the effective conjugation length. The layered macrocycle in the PMCDA series has a more flexible structure to enhance the dynamic motion of the rigid π-conjugated main chain. Therefore, the thermoresponsive gradual color-changing behavior is observed in a wide temperature range (-Fig. 3a–c). As the flexibility is tuned by the intercalated guests, the responsivity is different depending on the structures of the guest molecules. In addition, the flexible but confined PDA main chain with the linker ensures the appropriate stability of the original structures enabling the reversible color changes (Fig. 3a and b). In contrast, PLDA has a layered structure based on the densely packed linear amphiphilic DA monomers *via* van der Waals interaction. The layered structure is more rigid to induce the thermal motion in the wide temperature range. As the PDA main chain is not linked in the LDA series, the reversibility originating from the stability of the original structure is not achieved. In this manner, the layered macrocycles can be regarded as a new design concept providing the flexibility and tunability of dynamic properties based on the functional π-conjugated molecules.

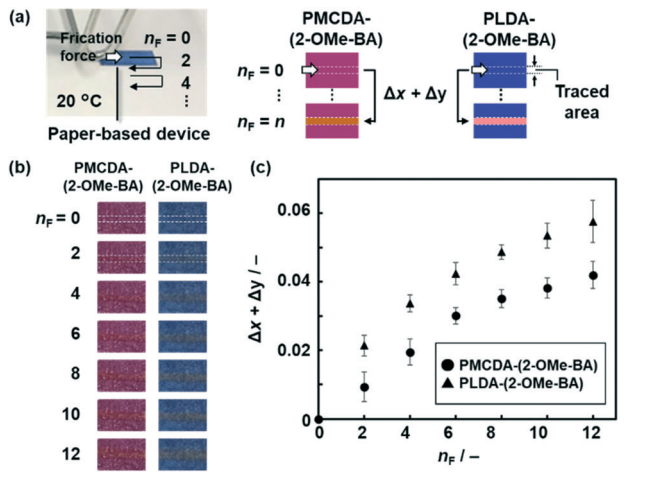

Fig. 4 Mechanoresponsive color-change properties of PMCDA-(2-OMe-BA) and PLDA-(2-OMe-BA). (a) Scheme for measurement of the color changes ($\Delta x + \Delta y$) with an increase in the amount of applied friction force (n_F). (b) Photographs of PMCDA-(2-OMe-BA) and PLDA-(2-OMe-BA) on filter paper with the application of a friction force of 7.07 N at each n_F. (c) Relationship between n_F and $\Delta x + \Delta y$.

Mechanoresponsive color-changing properties

In addition to the thermoresponsivity, PMCDA-(2-OMe-BA) and PLDA-(2-OMe-BA) showed the color change with the application of friction force (Fig. 4). A friction force of 7.07 N was applied to PMCDA-(2-OMe-BA) and PLDA-(2-OMe-BA) on filter paper (Fig. 4a). The changes in the red- and green-color intensity (Δx and Δy), the increment of x and y with respect to the original state, were calculated in the area of the traced line on the paper (Fig. 4a and b). According to our previous reports, the color change is not ascribed to the friction heat.[57,58] Fig. 4c shows the relationship between the amount of the applied friction force (n_F) and $\Delta x + \Delta y$. The color was gradually changed for both PMCDA-(2-OMe-BA) and PLDA-(2-OMe-BA) with an increase in n_F. On the other hand, the $\Delta x + \Delta y$ value of PMCDA-(2-OMe-BA) was smaller than that of PLDA-(2-OMe-BA) at the same n_F (Fig. 4c). This finding means that the responsivity of PMCDA-(2-OMe-BA) was lower than that of PLDA-(2-OMe-BA). The $\Delta x + \Delta y$ values are increased with an increase in n_F because the red-colored area is expanded. The color changes to red with the application of friction force correspond to the irreversible color transition observed with heating (Fig. 3). PMCDA-(2-OMe-BA) and PLDA-(2-OMe-BA) showed the irreversible color transition to red at 190 °C and 65 °C, respectively (Fig. 3b and c). This finding means that the flexible PMCDA-(2-OMe-BA) needs more stress to induce the irreversible color changes. Therefore, the responsivity of PMCDA-(2-OMe-BA) to the shear stress is lower than that of PLDA-(2-OMe-BA) (Fig. 4c). When weaker friction forces, such as 1.39 and 2.52 N, were applied to PMCDA-(2-OMe-BA), the $\Delta x + \Delta y$ values were smaller than those of 7.07 N at each n_F (Fig. S14 in the ESI†). The mechanoresponsivity is similar to that of the layered PLDA in our previous work.[58] In contrast, the stronger friction force (9.35 N) was not accurately visualized because the PMCDA-(2-OMe-BA) powder was removed from the paper substrates.

Application of the wide-range thermoresponsive color-changing properties

The gradual thermoresponsive color-changing properties of PMCDA-(2-OMe-BA) were applied to real-time temperature imaging (Fig. 5). Cryotherapy is a method for medical treatment of warts.[68,69] The affected part is immediately cooled with liquid nitrogen using a cotton bud or spray and then restored to body temperature. The relationship between the temperature changes and their effects is not fully clarified. Visualization of the temperature distribution and history around the affected part can be helpful for understanding the method. However, the temperature range is lower than that detectable using typical infrared thermography. In the present work, the temperature rising behavior after the cooling was visualized with the PMCDA-(2-OMe-BA)-coated paper (Fig. 5a), because the reversible color

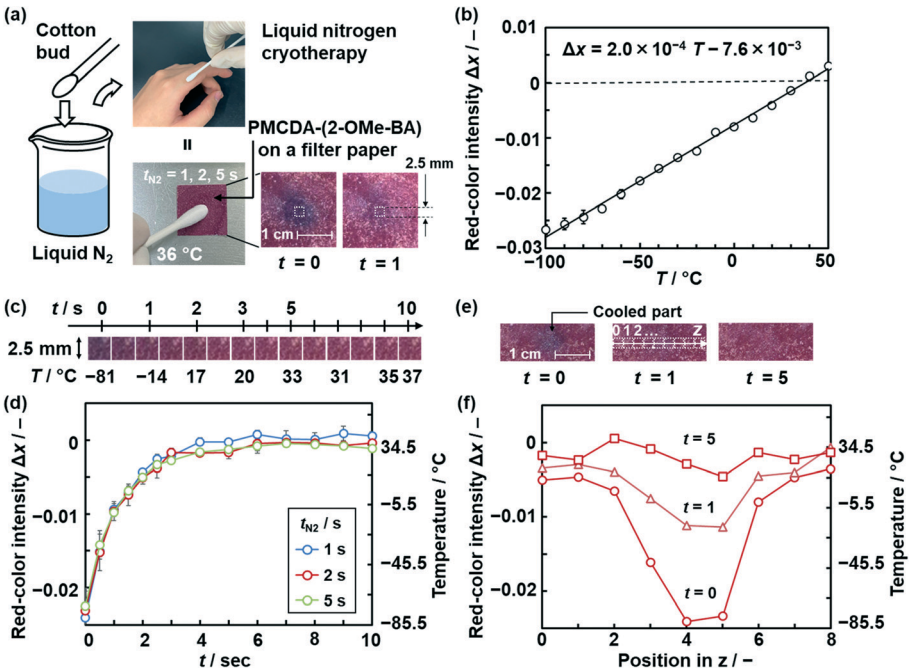

Fig. 5 Real-time temperature imaging during simulated liquid-nitrogen cryotherapy using the PMCDA-(2-OMe-BA) paper-based device. (a) Cooling of the PMCDA-(2-OMe-BA)-coated paper for t_{N_2} (1, 2, 5 s) using a cotton bud immersed in liquid nitrogen (N_2). (b) Calibration curve of the relationship between T and Δx. (c) Photographs of the color-changing behavior and temperature readings from the photographs using the approximation curve within t = 0–10 s. (d) Relationship between t and Δx (left axis) and relationship between t and T (right axis) for t_{N_2} = 1, 2, and 5 s. (e) Photographs of the paper-based device at t = 0, 1, and 5 s for t_{N_2} = 2 s. (f) Relationship between positions 1–8 in the z axis and Δx at t = 0, 1, and 5 s for t_{N_2} = 2 s.

changes were observed in the range of −100–190 °C (Fig. 3a and b and Table 1). An aqueous dispersion liquid containing MCDA-(2-OMe-BA) was filtered to collect the particles on a square piece of filter paper 2 cm length on each side. After the polymerization, the filter paper with coating of PMCDA-(2-OMe-BA) was obtained (Fig. 5a). The paper-based device was set on a temperature-controlled stage at 36 °C assumed as body temperature. A cotton bud was immersed in liquid nitrogen for *ca.* 10 s and then immediately pressed on the center part of the paper-based device with a contact area of 9.6 mm^2 for t_{N_2} = 1, 2, and 5 s. Then, the cotton bud was removed from the surface at t = 0. The processes including cooling and warming were recorded by a video camera. The image analysis was performed on the frames at certain t.

Prior to the temperature imaging, the calibration curve was prepared using the relationship between T and Δx (= $x - x_0$) within −100–50 °C (Fig. 5b), where x_0 is defined as x at 36 °C in this demonstration. The relationship was represented by a linear regression. The time-dependent color-change behavior was monitored at the central cooled part 2.5 mm square (Fig. 5c). The photographs indicate that the color of the cooled part was gradually changed from blue to purple within *ca.* 5 s (Fig. 5c and S15 in the ESI†). The average Δx values increased with an increase in t (Fig. 5d). The observed Δx values were converted to T using the calibration curve and its linear approximation formula (Fig. 5b and c). The Δx values in the left vertical axis are directly converted to T in the right vertical axis using the relationship based on the approximation formula (Fig. 5d). The warming behavior to 36 °C was not so different for t_{N_2}. The temperature distribution around the cooled part, namely positions 1–8 with square areas 2.5 mm in length, was studied using Δx in the z axis (Fig. 5e). The disappearance of the temperature gradient was visualized and quantified with an increase in t (Fig. 5e and f). In this manner, the temperature distribution in the range of −100–50 °C can be visualized by the characteristic color-changing properties of PMCDA-(2-OMe-BA). The device based on layered macrocycles enables temperature imaging in the range unsuitable for application of conventional infrared thermography.

Conclusions

Layered macrocycles were designed and synthesized as a new class of self-assembled functional soft materials. A designed macrocyclic monomer comprising functional, flexible linker, and intercalating units formed the self-assembled layered structures. Layered MCDA accommodated the guests in the interlayer space through intercalation. The topochemical polymerization provided the layered PMCDA with tunable stimuli-responsive color-changing properties depending on the guests. The PMCDA series showed thermoresponsive gradual color-changing properties in a wide temperature range (maximum at 330 K) with partial reversibility. The structural flexibility of the layered

macrocycles affords induction of the dynamic motion of the rigid π-conjugate moiety in a wide temperature range. The characteristic color-change properties were applied to real-time temperature imaging. The design strategy of the layered macrocycles, distinguished from conventional layered materials, can be applied to other soft materials for the emergence of dynamic functions based on intrinsically rigid π-conjugated macromolecules.

Author contributions

J. M. K. and Y. O. conceptualized and supervised this project with funding acquisition. J. M. H. and B. K. synthesized the MCDA monomer. N. S. carried out the experimental works and discussed the results with J. M. K. and Y. O. The original draft was prepared by N. S. and Y. O. The manuscript was reviewed and edited by all the authors.

Conflicts of interest

There are no conflicts to declare.

Acknowledgements

This work was partially supported by Asahi Glass Foundation (Y. Oaki) and AMED (Y. Oaki, JP21lm0203012j0003), and the National Research Foundation of Korea (2021R1A2C2005906 and 2021M3H4A1A02051834) (J.-M. Kim).

Notes and references

1 G. A. Ozin, *Adv. Mater.*, 1992, **4**, 612.
2 T. E. Mallouk and J. Gavin, *Acc. Chem. Res.*, 1998, **31**, 209.
3 A. Matsumoto, *Polym. J.*, 2003, **35**, 93.
4 J. Sakamoto, J. van Heijst, O. Lukin and A. D. Schlüter, *Angew. Chem., Int. Ed.*, 2009, **48**, 1030.
5 T. Govindaraju and M. B. Avinash, *Nanoscale*, 2012, **4**, 6102.
6 J. W. Colson and W. R. Dichtel, *Nat. Chem.*, 2013, **5**, 453.
7 K. Ariga, S. Watanabe, T. Mori and J. Takeya, *NPG Asia Mater.*, 2018, **10**, 90.
8 M. A. Solomos, F. J. Clairea and T. J. Kempa, *J. Mater. Chem. A*, 2019, **7**, 23537.
9 K. Ariga, E. Ahn, M. Park and B. S. Kim, *Chem. – Asian J.*, 2019, **14**, 2553.
10 C. N. R. Rao and K. Paramoda, *Bull. Chem. Soc. Jpn.*, 2019, **92**, 441.
11 G. Chakraborty, I. H. Park, R. Medishetty and J. J. Vittal, *Chem. Rev.*, 2021, **121**, 3751.
12 *Intercalation chemistry*, ed. M. S Whittingham and A. J. Jacobson, Academic Press, New York 1982.
13 M. Ogawa and K. Kuroda, *Chem. Rev.*, 1995, **95**, 399.
14 R. Schollhörn, *Chem. Mater.*, 1996, **8**, 1747.
15 E. Ruiz-Hitzky, M. Darder and P. Aranda, *J. Mater. Chem.*, 2005, **15**, 3650.
16 M. Osada and T. Sasaki, *Adv. Mater.*, 2012, **24**, 210.
17 V. Nicolosi, M. Chhowalla, M. G. Kanatzidis, M. S. Strano and J. N. Coleman, *Science*, 2013, **340**, 1226419.
18 H. P. Cong, J. F. Chen and S. H. Yu, *Chem. Soc. Rev.*, 2014, **43**, 7295.
19 X. Zhuang, Y. Mai, D. Wu, F. Zhang and X. Feng, *Adv. Mater.*, 2015, **27**, 403.
20 P. Ganter and B. V. Lotsch, *Mol. Syst. Des. Eng.*, 2019, **4**, 566.
21 Y. Oaki, *Chem. Commun.*, 2020, **56**, 13069.
22 Y. Oaki, *Chem. Lett.*, 2021, **50**, 305.
23 T. Kato, N. Mizoshita and K. Kishimoto, *Angew. Chem., Int. Ed.*, 2006, **45**, 38.
24 D. J. Broer, C. M. W. Bastiaansen, M. G. Debije and A. P. H. J. Schenning, *Angew. Chem., Int. Ed.*, 2012, **51**, 7102.
25 T. Kato, M. Yoshio, T. Ichikawa, B. Soberats, H. Ohno and M. Funahashi, *Nat. Rev. Mater.*, 2017, **2**, 17001.
26 A. Kuwabara, M. Enomoto, E. Hosono, K. Hamaguchi, T. Onuma, S. Kajiyama and T. Kato, *Chem. Sci.*, 2020, **11**, 10631.
27 K. Hamaguchi, R. Ichikawa, S. Kajiyama, S. Torii, Y. Hayashi, J. Kumaki, H. Katayama and T. Kato, *ACS Appl. Mater. Interfaces*, 2021, **13**, 20598.
28 T. Ogawa, *Prog. Polym. Sci.*, 1995, **20**, 943.
29 S. Okada, S. Peng, W. Spevak and D. Charych, *Acc. Chem. Res.*, 1998, **31**, 229.
30 R. W. Carpick, D. Y. Sasaki, M. S. Marcus, M. A. Eriksson and A. R. Burns, *J. Phys.: Condens. Matter*, 2004, **16**, R679.
31 M. A. Reppy and B. Piindzola, *Chem. Commun.*, 2007, 4317.
32 D. J. Ahn, S. Lee and J. M. Kim, *Adv. Funct. Mater.*, 2009, **19**, 1483.
33 X. Sun, T. Chen, S. Huang, L. Li and H. Peng, *Chem. Soc. Rev.*, 2010, **39**, 4244.
34 R. Jelinek and M. Ritenberg, *RSC Adv.*, 2013, **3**, 21192.
35 D. H. Park, B. J. Park and J. M. Kim, *Acc. Chem. Res.*, 2016, **49**, 1211.
36 J. Huo, Q. Deng, T. Fan, G. He, X. Hu, X. Hong, H. Chen, S. Luo, Z. Wang and D. Chen, *Polym. Chem.*, 2017, **8**, 7438.
37 X. Qian and B. Städler, *Chem. Mater.*, 2019, **31**, 1196.
38 M. Weston, A. D. Tjandra and R. Chandrawati, *Polym. Chem.*, 2020, **11**, 166.
39 B. Tieke, G. Lieser and G. Wegner, *J. Polym. Sci., Polym. Chem. Ed.*, 1979, **17**, 1631.
40 S. Lee and J. M. Kim, *Macromolecules*, 2007, **40**, 9201.
41 S. Dei, M. Matsumoto and A. Matsumoto, *Macromolecules*, 2008, **41**, 2467.
42 S. Ampornpun, S. Montha, G. Tumcharern, V. Vchirawongkwin, M. Sukwattanasinitt and S. Wacharasindhu, *Macromolecules*, 2012, **45**, 9038.
43 A. Chanakul, N. Traiphol and R. Traiphol, *J. Colloid Interface Sci.*, 2013, **389**, 106.
44 S. Lee, J. Lee, M. Lee, Y. K. Cho, J. Baek, J. Kim, S. Park, M. H. Kim, R. Chang and J. Yoon, *Adv. Funct. Mater.*, 2014, **24**, 3699.
45 K. P. Kooter, H. Jiang, S. Kolusheva, T. P. Vinod, M. Ritenberg, L. Zeiri, R. Volinsky, D. Malferrari, P. Galletti, E. Tagliavini and R. Jelinek, *ACS Appl. Mater. Interfaces*, 2014, **6**, 8613.
46 I. S. Park, H. J. Park, W. Jeong, J. Nam, Y. Kang, K. Shin, H. Chung and J. M. Kim, *Macromolecules*, 2016, **49**, 1270.

47 J. Huo, Q. Deng, T. Fan, G. He, X. Hu, X. Hong, H. Chen, S. Luo, Z. Wang and D. Chen, *Polym. Chem.*, 2017, **8**, 7436.
48 B. Hu, S. Sun, B. Wu and P. Wu, *Small*, 2019, **15**, 1804975.
49 N. Phonchai, C. Khanantong, F. Kielar, R. Traiphol and N. Traiphol, *ACS Appl. Nano Mater.*, 2019, **2**, 4489.
50 M. N. Tahir, A. Nyayachavadi, J. F. Morin and S. Rondeau-Gagné, *Polym. Chem.*, 2018, **9**, 3019.
51 R. Bisht, V. Dhyani and R. Jelinek, *Adv. Opt. Mater.*, 2021, **9**, 2001497.
52 J. M. Heo, Y. Kim, S. Han, J. F. Joung, S. H. Lee, S. Han, J. Noh, J. Kim, S. Park, H. Lee, Y. M. Choi, Y. S. Jung and J. M. Kim, *Macromolecules*, 2017, **50**, 900.
53 G. Shin, M. I. Khazi, U. Kundapur, B. Kim, Y. Kim, C. W. Lee and J. M. Kim, *ACS Macro Lett.*, 2019, **8**, 610.
54 K. Bae, J. M. Heo, M. I. Khazi, J. F. Joung, S. Park, Y. Kim and J. M. Kim, *Cryst. Growth Des.*, 2020, **20**, 434.
55 G. Shin, M. I. Khazi and J. M. Kim, *Macromolecules*, 2020, **53**, 149.
56 M. Okaniwa, Y. Oaki and H. Imai, *Adv. Funct. Mater.*, 2016, **26**, 3463.
57 Y. Ishijima, H. Imai and Y. Oaki, *Chem*, 2017, **3**, 509.
58 H. Terada, H. Imai and Y. Oaki, *Adv. Mater.*, 2018, **30**, 1801121.
59 K. Watanabe, H. Imai and Y. Oaki, *Small*, 2020, **16**, 2004586.
60 M. Nakamitsu, K. Oyama, H. Imai, S. Fujii and Y. Oaki, *Adv. Mater.*, 2021, **33**, 2008755.
61 J. M. Heo, Y. Son, S. Han, H. J. Ro, S. Jun, U. Kundapur, J. Noh and J. M. Kim, *Macromolecules*, 2019, **52**, 4405.
62 E. Reinhard, W. Heidrich, P. Debevec, S. Pattanaik, G. Ward and K. Myszkowski, *High Dynamic Range Imaging: Acquisition, Display, and Image-Based Lighting*, Elsevier Science, Saint Louis, 2nd edn, 2010, ch. 2, p. 35.
63 K. Tashiro, K. Ono, Y. Minagawa, M. Kobayashi, T. Kawai and K. Yosino, *J. Polym. Sci., Part B: Polym. Phys.*, 1991, **29**, 1223.
64 L. Rougeau, D. Picq, M. Rastello and Y. Frantz, *Tetrahedron*, 2008, **64**, 9430.
65 Y. Singh and N. Jayaraman, *Macromol. Chem. Phys.*, 2016, **217**, 940.
66 J. Huo, Z. Hu, G. He, X. Hong, Z. Yang, S. Luo, X. Ye, Y. Li, Y. Zhang, M. Zhang, H. Chen, T. Fan, Y. Zhang, B. Xiong, Z. Wang, Z. Zhu and D. Chen, *Appl. Surf. Sci.*, 2017, **423**, 951.
67 K. Watanabe, H. Imai and Y. Oaki, *J. Mater. Chem. C*, 2020, **8**, 1265.
68 J. C. Sterling, S. Gibbs, S. S. H. Hussain, M. F. M. Mustapa and S. E. Handfield-Jones, *Br. J. Dermatol.*, 2014, **171**, 696.
69 K. R. Soenjoyo, B. W. b. Chua, L. W. Y. Wee, M. J. A. Koh and S. B. Ang, *Dermatol. Ther.*, 2020, **33**, e14034.